Economic MPC for Online Least Costly Energy Management of Hybrid Electric Vehicles

Gabriele Pozzato[1,*], Matthias Müller[2], Simone Formentin[1], Sergio M. Savaresi[1]

[1] *Dipartimento di Elettronica, Informazione e Bioingegneria, Politecnico di Milano, Via G. Ponzio 34/5 20133 Milano, Italy*
e-mail: {gabriele.pozzato,simone.formentin,sergio.savaresi}@polimi.it

[2] *Institute of Automatic Control, Leibniz University Hannover, Germany*
e-mail: mueller@irt.uni-hannover.de

Abstract

In this work, the problem of online energy management of hybrid electric vehicles is addressed. A *least costly* objective function accounting for battery energy consumption and aging, and for the auxiliary power unit fuel consumption and noise emissions is considered. In this scenario, all the cost terms are expressed as monetary variables. This allows to assess the economic effectiveness of the proposed hybrid powertrain solution. Therefore, the online energy management policy is computed relying on the economic model predictive control framework. Some dissipativity properties for steady-state and periodic operation of the system under investigation are proved. Therefore, some results for close to optimum convergence of the economic model predictive control are provided. An electric bus case-study is illustrated in detail to show the performance of the proposed online management strategy.

Keywords: energy management, hybrid electric vehicle, economic model predictive control, dissipativity, differential inclusions

1. Introduction

In the last years, the quest for vehicular emissions reduction, fuel economy improvement, and energy efficiency have led automotive industries to devote time, effort, and money for the development of new powertrain solutions for the next generation of vehicles. In this scenario, Electric Vehicles (EVs) have become effective means for urban mobility thanks to the high efficiency, the absence of local emissions (Helmers and Marx (2012)), and the low price of the electrical energy. One of the obstacles limiting the spread of this technology is the low energy density of batteries if compared to carbon fuels (Warner (2015)), which leads to reduced all electric ranges. Thus, a common pathway to resolve this issue is the introduction of an auxiliary power unit called Range EXtender (REX). This device is composed of a diesel Internal Combustion Engine (ICE) coupled with an Electric Generator (EG). The internal combustion engine delivers mechanical power, which is converted into electrical power by the electric machine and then used for the vehicle motion. In this scenario, the architecture composed of the REX and the EV is a series hybrid electric powertrain (also known as Extended Range Electric Vehicle (EREV)) where two movers are available: the REX and the Li-ion battery.

It is widely recognized that, to evolve the standard ICE technology, hybrid electric vehicles come to hand. As a matter of fact, the introduction of multiple power sources allows for the improvement of the fuel economy and for the reduction of pollutants emissions (Sciarretta and Guzzella (2007)). However, to benefit from hybrid architectures it is of paramount importance to introduce effective Energy Management Strategies (EMSs) aiming at optimizing the power split between the available movers. In accordance with Onori et al. (2016), the EMS development may follow two principal routes: the *rule-based* one or the *model-based optimization* one. Rule-based strategies have been widely used for real-time implementation. In this scenario, heuristics are employed to choose the best control action at each time instant. The computational effort is reduced to its minimum, however, no optimality of the solution is guaranteed (see, *e.g.*, Jalil et al. (1997); Lin et al. (2001); Banvait et al. (2009)). In model-based optimization methods the EMS problem is recast as an optimal control problem. Therefore, the optimal energy management policy is retrieved minimizing a suitable objective function. To this end, different optimization methodologies can be adopted. Solutions based on dynamic programming are proposed by Pérez et al. (2006) and Sundstrom and Guzzella (2009). Moreover, in Murgovski et al. (2011, 2012b), and Elbert et al. (2014) solutions to the EMS problem based on convex programming tools are discussed. These policies are computed in a non-causal fashion and the optimization over the entire driving cycle is carried out offline. Eventually, real-time approximations of the non-causal optimal policies are obtained relying, *e.g.*, on the equivalent consumption minimization strategy, a Pontryagin's minimum principle-based heuristic (Musardo et al. (2005); Pisu and Rizzoni (2007)). The general drawback of model-based optimization approaches is the necessity to design a proper cost function with appropriate weights to balance the different cost terms.

In this work, the problem of online EMS development for hybrid electric vehicles is addressed. According to Pozzato et al. (2018, 2019, 2020), a *least costly* objective function is introduced. This formulation allows to express all the cost terms as monetary variables. Therefore, the solution of the EMS opti-

*Corresponding author.

mal control problem returns the overall vehicle operating cost, which is useful to assess the economic effectiveness of the proposed mobility solution. In this scenario, a control-oriented model for the EREV is first described. The REX provides power continuously and its usage is function of some idling heuristics. Then, the REX is characterized in terms of noise emissions, allowing for high penalization of unpleasant operating conditions. Thus, the EMS problem is formalized as a mixed-integer convex program with the battery modeled as a convex difference inclusion. The EMS problem is then solved online using an Economic Model Predictive Control (EMPC) framework. EMPC is a particular case of model predictive control where general, possibly economically motivated, performance criteria are considered (Faulwasser et al. (2018)). As usual in Model Predictive Control (MPC), the control input at each time step is computed by solving a finite-horizon optimal control problem and then applying the first component of the computed optimal predicted input sequence. In the context of economic MPC, dissipativity properties have turned out to play a crucial role[1]. Namely, dissipativity allows to characterize the optimal operating behavior of a system (with respect to the given performance criterion) and to analyze closed-loop convergence, compare Faulwasser et al. (2018); Müller et al. (2015). Available results in the literature establish dissipativity properties for certain types of difference equations (see, *e.g.*, Damm et al. (2014); Berberich et al. (2020)).

Against this background, the paper is not only focused on providing an EMPC solution for the EMS problem of EREVs, but also to derive dissipativity properties that allow to conclude closed-loop performance and convergence results of EMPC schemes for more general system classes. Therefore, the main innovative contributions of the paper are summarized as follows:

- On the one hand, considering generic dynamical systems described by convex difference inclusions (which include also the battery energy model (23) of the EMS problem), dissipativity is proven for both cases of optimal steady-state and periodic operation. Proving this property allows to retrieve important information on the performance of a generic EMPC for such systems;
- On the other hand, the implications of the aforementioned dissipativity results for the EMS problem at hand are assessed. Moreover, for the first time the online least costly solution is computed rewriting the EMS problem in the EMPC framework. This allows to obtain an online energy management strategy with convergence guarantees given by dissipativity.

The remainder of the paper is organized as follows. First, in Section 2 a backward powertrain model is introduced. Therefore, Section 3 describes the energy management strategy problem for the EREV. Then, theoretical results on dissipativity for steady-state and periodic operation of systems modeled by convex difference inclusions are discussed in Section 4. In Section 5, the validity of such dissipativity conditions and of their implications is shown, in a simulation environment, for the particular case of an extended range electric bus. Finally, in Section 6 some final remarks are carried out.

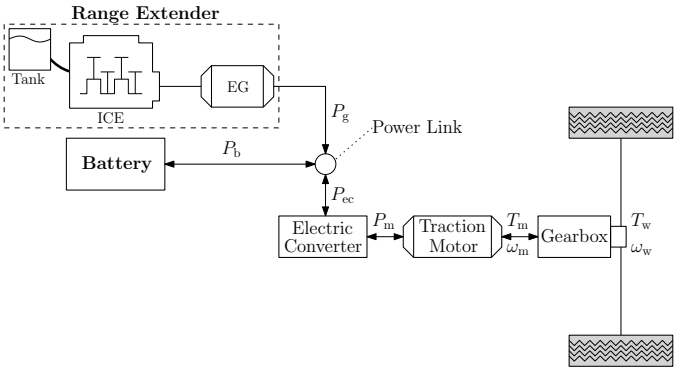

Figure 1: EREV powertrain configuration.

2. Powertrain Modeling

In this section, a convex control-oriented model for the powertrain components is described in detail (Figure 1). Relying on a pure backward paradigm, the behavior of the vehicle is simulated from driving cycle speed (v) and slope (θ) profiles, computing the upstream power flows. This modeling strategy is well established in the literature and provides a robust and reliable tool to analyze the power split in hybrid powertrains (Onori et al. (2016)). For clarity, the modeling is proposed in continuous time and time dependencies are neglected till the end of the section.

Vehicle dynamics. The vehicle motion is described considering only the longitudinal dynamics. The equilibrium of forces and moments leads to the following balance equation (Onori et al. (2016)):

$$T_{\mathrm{w}} = R_{\mathrm{w}}(M\dot{v} + F_{\mathrm{b}} + F_{\mathrm{f}}), \quad \omega_{\mathrm{w}} = \frac{v}{R_{\mathrm{w}}} \tag{1}$$

where M is the vehicle mass, T_{w} and ω_{w} respectively the wheel torque and rotational speed, and R_{w} the wheel radius. The dot operator denotes the first order derivative with respect to time. F_{b} is the mechanical braking force. The friction force F_{f} takes the following expression (Rajamani (2011)):

$$F_{\mathrm{f}} = Mg\sin(\theta) + C_{\mathrm{r}}Mg\cos(\theta) + \frac{1}{2}\rho_{\mathrm{a}}AC_{\mathrm{x}}v^2 \tag{2}$$

with g the gravitational acceleration, ρ_{a} the air density, and A the vehicle reference area. C_{r} and C_{x} are the roll and drag coefficients, respectively.

Gearbox. Traction motor and wheels are connected by means

[1] Providing a high-level physical interpretation, a system is dissipative if its increase in energy storage is no more than the supplied energy from outside to the system (Brogliato et al. (2007)).

of a constant ratio transmission (Onori et al. (2016)):

$$T_{\mathrm{m}} = \begin{cases} \frac{1}{r_{\mathrm{t}}\eta_{\mathrm{t}}} T_{\mathrm{w}}, & \text{if } T_{\mathrm{w}} \geq 0 \text{ (traction)} \\ \frac{\eta_{\mathrm{t}}}{r_{\mathrm{t}}} T_{\mathrm{w}}, & \text{if } T_{\mathrm{w}} < 0 \text{ (braking)} \end{cases} \qquad (3)$$
$$\omega_{\mathrm{m}} = r_{\mathrm{t}}\omega_{\mathrm{w}}$$

where T_{m} is the motor torque, ω_{m} the motor rotational speed, r_{t} the gear ratio, and η_{t} the transmission efficiency.

Traction motor. The torque is provided by the traction motor, which is modeled as an efficiency map (Murgovski et al. (2012a)). Thus, the electric power P_{m} in motor and generator modes takes the following expression:

$$P_{\mathrm{m}} = \begin{cases} \frac{T_{\mathrm{m,i}}\omega_{\mathrm{m}}}{\eta_{\mathrm{m}}(T_{\mathrm{m,i}},\omega_{\mathrm{m}})}, & \text{if } T_{\mathrm{m,i}} \geq 0 \text{ (motor)} \\ T_{\mathrm{m,i}}\omega_{\mathrm{m}}\eta_{\mathrm{m}}(T_{\mathrm{m,i}},\omega_{\mathrm{m}}), & \text{if } T_{\mathrm{m,i}} < 0 \text{ (generator)} \end{cases} \qquad (4)$$
$$T_{\mathrm{m,i}} = T_{\mathrm{m}} + J_{\mathrm{m}}\dot{\omega}_{\mathrm{m}}$$

where J_{m} is the motor inertia and η_{m} the efficiency.

Electric converter. The power electronics in between the battery, the REX, and the traction motor is modeled as an average efficiency η_{ec} (Hu et al. (2013)):

$$P_{\mathrm{ec}} = \begin{cases} \frac{P_{\mathrm{m}}}{\eta_{\mathrm{ec}}}, & \text{if } P_{\mathrm{m}} \geq 0 \\ P_{\mathrm{m}}\eta_{\mathrm{ec}}, & \text{if } P_{\mathrm{m}} < 0 \end{cases} \qquad (5)$$

where P_{ec} is the power requested by the driving cycle.

Power link. The electric power is supplied by two competing power sources: the battery and the REX. Thus, the total power required by the drivetrain must satisfy the following balance equation (see Onori et al. (2016)): $P_{\mathrm{ec}} = P_{\mathrm{b}} + P_{\mathrm{g}}$. P_{g} is the REX generated power and P_{b} the absorbed/supplied battery power.

Battery. Depending on the specifications for the nominal voltage and capacity (Warner (2015)), a battery pack is composed of cells disposed in a series/parallel configuration. Neglecting the voltage dynamics, the battery power takes the following expression:

$$P_{\mathrm{b}} = v_{\mathrm{b}} i_{\mathrm{b}} = (v_{\mathrm{oc}} - R_{\mathrm{b}} i_{\mathrm{b}}) i_{\mathrm{b}} \qquad (6)$$

where i_{b} is the battery current and R_{b} the battery pack internal resistance. v_{oc} is the open circuit voltage which is approximated as an affine function of the State of Charge (SoC) (Guzzella et al. (2007)):

$$v_{\mathrm{oc}} = A_{\mathrm{b}}\mathrm{SoC} + B_{\mathrm{b}}. \qquad (7)$$

A_{b} and B_{b} are obtained experimentally, fitting a real-world open circuit voltage, more specifically the Li-ion cell A123 ANR266 50M1-B. Therefore, solving (6) for the battery current leads to:

$$i_{\mathrm{b}} = \frac{v_{\mathrm{oc}} - \sqrt{v_{\mathrm{oc}}^2 - 4R_{\mathrm{b}}P_{\mathrm{b}}}}{2R_{\mathrm{b}}}. \qquad (8)$$

According to Guzzella et al. (2007), the battery SoC takes the following expression:

$$\dot{\mathrm{SoC}} = -\frac{i_{\mathrm{b}}}{Q_{\mathrm{b}}} \qquad (9)$$

where Q_{b} is the battery capacity. During their lifetime, batteries experience aging, which leads to a capacity degradation. Thus, to account for the aging phenomena, the following simplified model is introduced:

$$\dot{\mathrm{SoH}} = \frac{\sigma_{\mathrm{b}}}{N_{\mathrm{b}}Q_{\mathrm{b}}V_{\mathrm{b}}}|P_{\mathrm{b}}|. \qquad (10)$$

SoH denotes the battery State of Health; growing from 0 to 1 proportionally to the kWh−throughput (*i.e.*, SoH = 0 and SoH = 1 denote the healthy and dead battery, respectively). N_{b} is the battery life cycle (defined as the number of charges plus the number of discharges), and V_{b} the battery nominal voltage. The severity factor σ_{b} is modeling the battery usage away from nominal conditions. In accordance with Serrao et al. (2011), this factor is a function of C-rate and temperature. Assuming to work around nominal conditions and between 20-35 (°C), a constant severity factor is considered (Guanetti et al. (2016)).

Battery convex model. In this paper, the EMS problem is solved relying on convex programming tools, which requires the model of the system to be defined as a set of convex constraints. The aforementioned battery model is non-convex. Thus, a reformulation with respect to the battery energy E is introduced (Elbert et al. (2014)):

$$\dot{E} = \phi(E, P_{\mathrm{b}}, P_{\mathrm{ec}}) = -\frac{A_{\mathrm{b}}}{R_{\mathrm{b}}Q_{\mathrm{b}}}(E + E_0) + \frac{A_{\mathrm{b}}}{R_{\mathrm{b}}Q_{\mathrm{b}}}\sqrt{(E+E_0)^2 - \frac{2R_{\mathrm{b}}Q_{\mathrm{b}}}{A_{\mathrm{b}}}P_{\mathrm{b}}(E+E_0)} \qquad (11)$$

where $E_0 = \frac{Q_{\mathrm{b}}}{2A_{\mathrm{b}}}B_{\mathrm{b}}^2$. Equation (11) is still non-convex. Given the concavity of the term on the right hand side of (11), the battery internal energy dynamic model is relaxed introducing the following differential inclusion:

$$\dot{E} \in \Phi(E, P_{\mathrm{b}}, P_{\mathrm{ec}}) = \{y \in \mathbb{R} | y \leq \phi(E, P_{\mathrm{b}}, P_{\mathrm{ec}})\} \qquad (12)$$

where Φ is the *hypograph* of ϕ: a convex set due to the concavity of ϕ (Boyd and Vandenberghe (2004)). To ensure the non-negativity of the term inside the square root, the following inequality must be satisfied:

$$P_{\mathrm{b}} \leq (E + E_0)\frac{A_{\mathrm{b}}}{2Q_{\mathrm{b}}R_{\mathrm{b}}}. \qquad (13)$$

Given an objective function accounting for battery energy usage (as in this work), the relaxation (12) does not prejudice the accuracy of the solution. As a matter of fact, in case of optimal solution, (12) holds with equality (Elbert et al. (2014)). This is reasonable because any solution holding with strict inequality would be associated to a waste of battery energy and therefore to a suboptimal usage of the power split.

Range extender. The limited all electric range of electric vehicles is a major concern in the automotive industry. Therefore, to extend the vehicle driving range a possible solution is the introduction of REXs. In this paper, the REX is a device composed of a diesel ICE coupled with an EG. Hence, the mechanical power generated by the ICE is converted into electrical power and used to provide energy to the electric drivetrain.

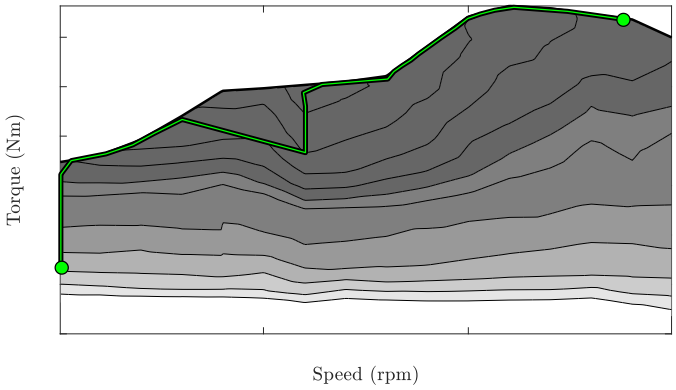

Figure 2: Combined ICE+EG efficiency map as function of ICE rotational speed and torque. The maximum efficiency path is shown. Due to confidentiality reasons, figure axes labels are removed.

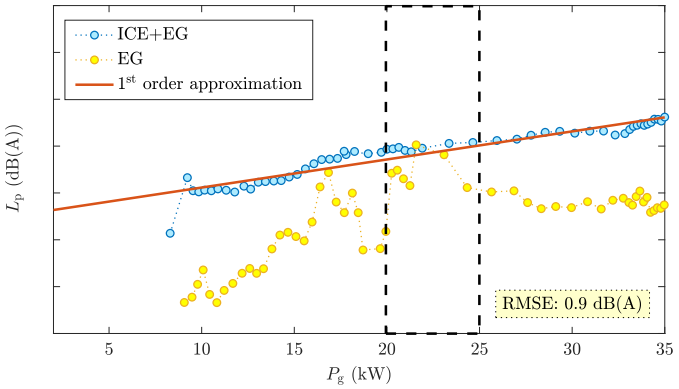

Figure 3: REX sound pressure levels. ICE+EG noise emissions data are shown together with the SPL first order approximation. Critical frequencies are highlighted by the rectangle. Due to confidentiality reasons, y-axis label is removed.

Power generation. According to Pozzato et al. (2020), the REX is modeled as a quasi-static device in which the relationship between fuel and generated power is given by a combined efficiency map of ICE and EG (Figure 2). The electric generated power takes values in the following range:

$$2 \leq P_g \leq 35 \cup 0 \ (\text{kW}). \tag{14}$$

If the REX is idling, P_g is equal to 0 (kW). Clearly, a power request can be actuated at different REX (torque,speed) operating points. Therefore, the REX is assumed to work at the maximum possible efficiency, *i.e.*, given a certain power request, among all the possible (torque,speed) actuation scenarios the highest efficiency point is chosen. This leads to the maximum efficiency path shown in Figure 2. Denoting by $\eta_g(P_g)$ the REX maximum efficiency, fuel thermal power (P_f) and rate ($\dot{m}_f$) are modeled as follows:

$$P_f = \frac{P_g}{\eta_g(P_g)}, \qquad \dot{m}_f = \frac{P_f}{\lambda_f} \tag{15}$$

where λ_f is the fuel lower heating value. The fuel thermal power is approximated by a second order polynomial function (Murgovski et al. (2012b)):

$$P_f = A_g P_g^2 + B_g P_g + C_g \tag{16}$$

in which A_g, B_g, and C_g are identified parameters. If the power request is higher than P_{thr}, the REX provides power to the traction motor. Conversely, if the power request is smaller than P_{thr}, the REX idles. This behavior is modeled as follows:

$$q(P_{ec}) = \begin{cases} 1, & P_{ec} > P_{thr} \\ 0, & \text{otherwise.} \end{cases} \tag{17}$$

Moreover, the maximum power $\overline{P_g}(\overline{\vartheta}) = 35$ (kW) is provided only if the REX is warmed-up. As a matter of fact, because of sub-optimal lubricant and component temperatures, the ICE thermal efficiency is significantly lower at cold-start if compared to when the vehicle reaches steady-state conditions (Roberts et al. (2014)). Therefore, once the vehicle is turned on, for the first 6 (min) of operation, *i.e.*, the time needed to warm-up the engine, the maximum power is limited to $\overline{P_g}(\underline{\vartheta}) = 27$ (kW). Eventually, the possible REX operating conditions are summarized as follows:

$$\begin{cases} q(P_{ec})\underline{P_g} \leq P_g \leq q(P_{ec})\overline{P_g}(\underline{\vartheta}), & \text{warm-up phase} \\ q(P_{ec})\underline{P_g} \leq P_g \leq q(P_{ec})\overline{P_g}(\overline{\vartheta}), & \text{warmed-up engine} \end{cases} \tag{18}$$

where $\underline{P_g}$ is the minimum electric power which can be generated by the REX.

Noise modeling. According to Pozzato et al. (2020), noise emissions are characterized by Sound Pressure Levels (SPLs) measured at 1 (m) distance from the source. Thus, sound levels are then A-weighted and expressed in dB(A) in order to account for the varying human's ear sensitivity in the audible frequency range (Cory (2010)). As shown by Figure 3, noise emission measurements for the combined scenario (ICE+EG) are available and mapped as function of the REX generated power. Therefore, the following simplified model is created fitting the acquired data with a first order polynomial function:

$$L_p = A_{SPL} P_g + B_{SPL} \tag{19}$$

where A_{SPL} and B_{SPL} are identified parameters, and B_{SPL} models the noise emitted while the REX is idling. The approximation leads to a Root Mean Square Error (RMSE) of 0.9 (dB(A)). Unfortunately, the noise emitted by the EG becomes annoying, in terms of psychoacoustics (Zwicker and Fastl (2013)), between 20 and 25 (kW). Consequently, in the next section a noise emissions weighting factor, varying with the REX generated power, is proposed.

3. Energy Management Problem Formulation

The goal of the EMS is to optimally split the power request between the available movers, *i.e.*, the battery pack and the REX, minimizing a suitable objective function. First the battery model (11) is discretized, then, the EMS problem is formalized as a discrete time optimal control problem over a finite time horizon N.

3.1. Discretized Battery Energy Model

The battery internal energy is chosen as the state variable. Thus, forward Euler differentiation is employed to obtain the discretized model from (11):

$$E(k+1) = E(k) - T_\mathrm{s}\frac{A_\mathrm{b}}{Q_\mathrm{b}R_\mathrm{b}}(E(k)+E_0)+ T_\mathrm{s}\frac{A_\mathrm{b}}{Q_\mathrm{b}R_\mathrm{b}}\sqrt{(E(k)+E_0)^2 - \frac{2R_\mathrm{b}Q_\mathrm{b}}{A_\mathrm{b}}(P_\mathrm{b}(k)+P_\mathrm{cool})(E(k)+E_0)} \tag{20}$$

where the constant P_cool is explicitly modeling the power supplied by the battery to keep its own temperature to an optimal reference (according to Corno and Pozzato (2019), usually around 30-35 (°C)) and T_s is the sampling time. Far from the SoC upper and lower bounds, (20) is well approximated by a model expressed in terms of the battery energy difference ΔE:

$$\Delta E(k+1) = f(\Delta E(k), P_\mathrm{b}(k), P_\mathrm{ec}(k)) = -T_\mathrm{s}\frac{A_\mathrm{b}}{R_\mathrm{b}Q_\mathrm{b}}(\Delta E(k)+E_0)+ T_\mathrm{s}\frac{A_\mathrm{b}}{R_\mathrm{b}Q_\mathrm{b}}\sqrt{(\Delta E(k)+E_0)^2 - \frac{2R_\mathrm{b}Q_\mathrm{b}}{A_\mathrm{b}}(P_\mathrm{b}(k)+P_\mathrm{cool})(\Delta E(k)+E_0)}. \tag{21}$$

Therefore, at each time instant k, the battery energy is computed with the following cumulative sum:

$$E(k) = E(0) + \sum_{\iota=0}^{k}\Delta E(\iota) \tag{22}$$

where $E(0)$ is the battery internal energy initial condition. The model introduced by (21) and (22) is not equivalent to (20). As a matter of fact, in the general case, (21) is also a function of the battery energy state E. However, E is at least one order of magnitude smaller than E_0 in all its feasible domain (*i.e.*, for $\mathrm{SoC} \in \left[\underline{\mathrm{SoC}}, \overline{\mathrm{SoC}}\right]$). Thus, the error introduced by the approximation (21) is negligible. For instance, let us consider any SoC initial condition in the range $[25,75]\%$ (for which a $\mathrm{SoC} > 0$ is guaranteed over the considered time horizon of 200 seconds) and a constant battery power request of 220 (kW). In this scenario, the average error between the two modeling strategies, in terms of final state of charge, is 0.015%. Since the right hand side of (21) is still concave, the convex model is obtained introducing the *hypograph* reformulation (analogously to (12)), leading to the following difference inclusion:

$$\begin{aligned}\Delta E(k+1) \in F(\Delta E, P_\mathrm{b}, P_\mathrm{ec}) = \\ = \{y \in \mathbb{R} | y \leq f(\Delta E(k), P_\mathrm{b}(k), P_\mathrm{ec}(k))\}.\end{aligned} \tag{23}$$

Eventually, (21) fits well with the proposed EMS formulation. As a matter of fact, the optimal battery operation is a function of ΔE and not of E. This is reasonable since, far away from the SoC bounds, the power supplied/absorbed by the battery pack is always bounded between $\left[\underline{P_\mathrm{b}}, \overline{P_\mathrm{b}}\right]$, independent of the actual SoC state. Moreover, (23) shows to be a smart reformulation which allows to assess the dissipativity properties of the system (as shown in Section 5).

3.2. Optimal Control Problem

The REX generated power P_g and the battery power P_b are the control variables satisfying the following condition $P_\mathrm{ec}(k) \leq P_\mathrm{b}(k) + P_\mathrm{g}(k)$. The inequality models the possibility to dissipate electric energy in a braking resistor (which is however not an optimal policy). P_ec and $q(P_\mathrm{ec})$ (computed as in (17)) are exogenous inputs. Thus, the mixed-integer convex program reads as follows:

$$\begin{aligned}\underset{\Delta E, P_\mathrm{g}, P_\mathrm{b}}{\text{minimize}} \quad & -\frac{\alpha_\epsilon}{\eta_\mathrm{grid}}\Delta E(N) + \Big\} V_\mathrm{f} \\ & T_\mathrm{s}\sum_{k=0}^{N-1}\frac{\alpha_\epsilon}{\eta_\mathrm{grid}}\frac{-\Delta E(k)}{T_\mathrm{s}} + \Big\} l_1 \\ & T_\mathrm{s}\sum_{k=0}^{N-1}\beta_\epsilon\frac{\sigma_\mathrm{b}}{N_\mathrm{b}} \mid P_\mathrm{b}(k) + P_\mathrm{cool} \mid + \\ & T_\mathrm{s}\sum_{k=0}^{N-1}\gamma_\epsilon(A_\mathrm{g}P_\mathrm{g}(k)^2 + B_\mathrm{g}P_\mathrm{g}(k) + C_\mathrm{g}) + \\ & T_\mathrm{s}\sum_{k=0}^{N-1}\delta_{\epsilon,0}\mathrm{SF}(v)\Big[(A_\mathrm{SPL}P_\mathrm{g}^{(1)}(k) + B_\mathrm{SPL}) + \\ & \qquad (2A_\mathrm{SPL}P_\mathrm{g}^{(2)}(k) + q_\mathrm{SPL}^{(1)}(k)B_\mathrm{SPL}) + \\ & \qquad (A_\mathrm{SPL}P_\mathrm{g}^{(3)}(k) - q_\mathrm{SPL}^{(2)}(k)B_\mathrm{SPL})\Big] \Big\} l_2\end{aligned} \tag{24}$$

subject to

$$\begin{aligned}&\Delta E(k+1) \in F(\Delta E, P_\mathrm{b}, P_\mathrm{ec}) = \\ &\qquad = \{y \in \mathbb{R} | y \leq f(\Delta E(k), P_\mathrm{b}(k), P_\mathrm{ec}(k))\} \\ &P_\mathrm{ec}(k) \leq P_\mathrm{b}(k) + P_\mathrm{g}(k) \\ &\underline{\Delta E} \leq \Delta E(k) \leq \overline{\Delta E} \\ &\underline{P_\mathrm{b}} \leq P_\mathrm{b}(k) \leq \overline{P_\mathrm{b}} \\ &P_\mathrm{b}(k) \leq (\Delta E(k) + E_0)\frac{A_\mathrm{b}}{2Q_\mathrm{b}R_\mathrm{b}} - P_\mathrm{cool} \\ &\begin{cases} q(P_\mathrm{ec})\underline{P_\mathrm{g}} \leq P_\mathrm{g}(k) \leq q(P_\mathrm{ec})\overline{P_\mathrm{g}}(\underline{\vartheta}), & \text{warm-up phase} \\ q(P_\mathrm{ec})\underline{P_\mathrm{g}} \leq P_\mathrm{g}(k) \leq q(P_\mathrm{ec})\overline{P_\mathrm{g}}(\overline{\vartheta}), & \text{warmed-up engine} \end{cases} \\ &p_\mathrm{g}^{(1)}q_\mathrm{SPL}^{(1)}(k) \leq P_\mathrm{g}^{(1)}(k) \leq p_\mathrm{g}^{(1)} \\ &(p_\mathrm{g}^{(2)} - p_\mathrm{g}^{(1)})q_\mathrm{SPL}^{(2)}(k) \leq P_\mathrm{g}^{(2)}(k) \leq q_\mathrm{SPL}^{(1)}(k)(p_\mathrm{g}^{(2)} - p_\mathrm{g}^{(1)}) \\ &0 \leq P_\mathrm{g}^{(3)}(k) \leq q_\mathrm{SPL}^{(2)}(k)(\overline{P_\mathrm{g}}(\overline{\vartheta}) - p_\mathrm{g}^{(2)})\end{aligned} \tag{25}$$

Thus, the following initial condition is introduced:

$$\Delta E(0) = 0 \text{ (kJ)}.$$

The cost function (24) is composed of four different terms. First, the electrical energy needed to replace the battery charge depleted during the driving cycle is modeled by:

$$J_\mathrm{e} = -\frac{\alpha_\epsilon}{\eta_\mathrm{grid}}\Delta E(N) + T_\mathrm{s}\sum_{k=0}^{N-1}\frac{\alpha_\epsilon}{\eta_\mathrm{grid}}\frac{-\Delta E(k)}{T_\mathrm{s}} \tag{26}$$

where α_ϵ is the cost of 1 (kWh) of grid energy and $\Delta E(N)$ is the terminal condition. The minus sign in front of ΔE is introduced because, in correspondence of a negative variation of the battery

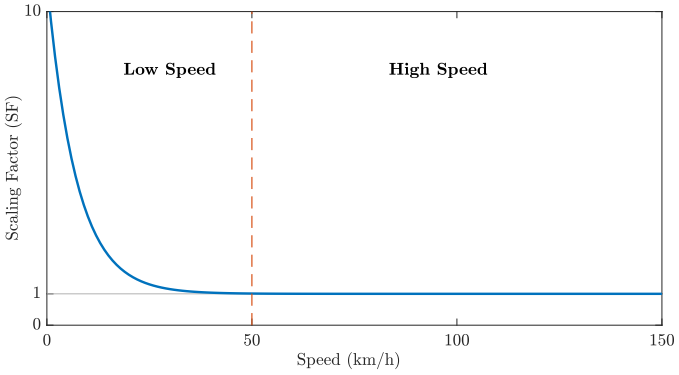

Figure 4: SF as function of vehicle speed. High vehicle speeds lead to lower noise penalization.

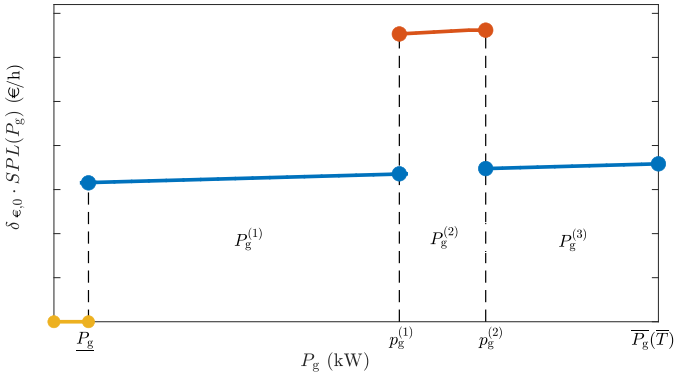

Figure 5: Noise cost, piecewise affine model. Due to confidentiality reasons, y-axis labels are removed.

internal energy (*i.e.*, while the SoC is decreasing), the monetary cost must increase because more energy is needed to recharge the battery. Then, the portion of battery life cycle throughput depleted along the driving cycle is described as:

$$J_a = T_s \sum_{k=0}^{N-1} \beta_€ \frac{\sigma_b}{N_b} \mid P_b(k) + P_{cool} \mid \tag{27}$$

with $\beta_€$ the purchase cost of 1 (kWh) of battery capacity. Thus, the REX fuel consumption is modeled as follows:

$$J_f = T_s \sum_{k=0}^{N-1} \gamma_€ (A_g P_g(k)^2 + B_g P_g(k) + C_g) \tag{28}$$

where $\gamma_€$ is the price for 1 (kWh) of fuel energy. The noise cost is expressed by the following term:

$$\begin{aligned} J_n &= T_s \sum_{k=0}^{N-1} \delta_{€,0} \mathrm{SF}(v)\ SPL(P_g) = \\ &= T_s \sum_{k=0}^{N-1} \delta_{€,0} \mathrm{SF}(v) \Big[(A_{\mathrm{SPL}} P_g^{(1)}(k) + B_{\mathrm{SPL}}) + \\ &\qquad (2A_{\mathrm{SPL}} P_g^{(2)}(k) + q_{\mathrm{SPL}}^{(1)}(k) B_{\mathrm{SPL}}) + \\ &\qquad (A_{\mathrm{SPL}} P_g^{(3)}(k) - q_{\mathrm{SPL}}^{(2)}(k) B_{\mathrm{SPL}}) \Big] \end{aligned} \tag{29}$$

with $\delta_{€,0}$ the baseline cost for the REX noise emissions and $\mathrm{SF}(v)$ a scaling factor function of the vehicle speed v (Figure 4). $\mathrm{SF}(v)$ is introduced in order to increase the noise penalization for low vehicle speeds, where the background noise is absent. Therefore, the noise cost is modeled by the piecewise affine function within square brackets of (29) (pictorially represented by Figure 5) and the following set of inequalities:

$$\begin{aligned} p_g^{(1)} q_{\mathrm{SPL}}^{(1)}(k) &\le P_g^{(1)}(k) \le p_g^{(1)} \\ (p_g^{(2)} - p_g^{(1)}) q_{\mathrm{SPL}}^{(2)}(k) &\le P_g^{(2)}(k) \le q_{\mathrm{SPL}}^{(1)}(k)(p_g^{(2)} - p_g^{(1)}) \\ 0 &\le P_g^{(3)}(k) \le q_{\mathrm{SPL}}^{(2)}(k)(\overline{P_g}(\overline{\vartheta}) - p_g^{(2)}) \end{aligned} \tag{30}$$

with $q_{\mathrm{SPL}}^{(1)}, q_{\mathrm{SPL}}^{(2)}$ and $P_g^{(1)}, P_g^{(2)}, P_g^{(3)}$ binary and real variables, respectively. The introduction of integer variables allows to select in which of three regions, highlighted in Figure 5, the range extender is working. Therefore, P_g takes the following expression:

$$P_g(k) = P_g^{(1)}(k) + P_g^{(2)}(k) + P_g^{(3)}(k). \tag{31}$$

To simplify the notation, in (24) and (25), P_g is used when possible. As already mentioned, a higher cost is applied to generated powers between $p_g^{(1)} = 20$ and $p_g^{(2)} = 25$ (kW), which are critical from a psychoacoustics viewpoint. The selection of $\delta_{€,0}$ is arbitrary and should be carefully made in order to account for the negative impact of loud and long-lasting noises on people's health and productivity, and on the natural environment. According to Pozzato et al. (2020), a value of 0.018 $(€\mathrm{dB(A)}^{-1}\mathrm{h}^{-1})$ is a reasonable choice.

The presence of both integer and real valued variables leads to mixed-integer convex problem which can be solved relying on mixed integer convex programming tools[2]. The application parameters are listed in Table 1.

4. Economic MPC and Dissipativity for Convex Difference Inclusions

As was shown recently, (strict) dissipativity can be employed to characterize the optimal operating conditions of a given system. In particular, this is possible for the cases of optimal steady-state and optimal periodic operation (Müller et al. (2015); Zanon et al. (2017); Faulwasser et al. (2018)). Furthermore, the same (strict) dissipativity conditions can in turn be employed to establish convergence to the optimal operating behavior of the closed-loop system resulting from application of economic MPC schemes (Müller and Grüne (2016); Zanon et al. (2017); Faulwasser et al. (2018)). Given this crucial role for obtaining closed-loop performance and convergence guarantees, proving dissipativity is of importance also beyond the context of the energy management, which is why the following results are proved for general nonlinear, convex, difference inclusions (which include as a special case the considered battery energy

[2]The solver *Gurobi* (version 8) is employed (`http://www.gurobi.com`). Solutions of the optimal control problem were computed on a Intel Core i7-7700HQ processor with 16.0 (GB) of RAM.

Table 1: Application parameters.

Variable	Description	Unit	Value
Vehicle			
g	Gravitational acceleration	$(\mathrm{m/s^2})$	9.81
M	Vehicle mass (with battery pack)	(kg)	12635
R_w	Wheel radius (Hu et al. (2013))	(m)	0.509
C_r	Rolling coefficient (Hu et al. (2013))	$(-)$	0.007
C_x	Drag coefficient (Hu et al. (2013))	$(-)$	0.7
A	Vehicle reference area (Hu et al. (2013))	$(\mathrm{m^2})$	7.540
η_t	Transmission efficiency (Hu et al. (2013))	$(-)$	0.97
r_t	Gear ratio (Hu et al. (2013))	$(-)$	4.7
J_m	Electric motor inertia (Hu et al. (2015))	$(\mathrm{kg\ m^2})$	2.3
η_ec	Electric converter efficiency (Hu et al. (2013))	$(-)$	0.98
ρ_a	Air density (Hu et al. (2013))	$(\mathrm{kg/m^3})$	1.184
Battery			
A_b	Voltage parameter	(V)	27.10
B_b	Voltage parameter	(V)	585.951
V_b	Nominal voltage	(V)	600
Q_b	Nominal capacity	(Ah)	107
N_b	Nominal life cycle	$(-)$	4000
σ_b	Severity factor (20-35 (°C)) (Suri and Onori (2016))	$(-)$	0.95
η_grid	Charging efficiency (Xiong et al. (2009))	$(-)$	0.92
P_cool	Cooling power (Corno and Pozzato (2019))	(kW)	0.6
$\overline{P_\mathrm{b}}$	Maximum power (Hu et al. (2013))	(kW)	220
$\underline{P_\mathrm{b}}$	Minimum power (Hu et al. (2013))	(kW)	-220
$\overline{\mathrm{SoC}}$	Maximum SoC	(%)	80
$\underline{\mathrm{SoC}}$	Minimum SoC	(%)	20
$\overline{\Delta E}$	Maximum ΔE	(kJ)	216.8
$\underline{\Delta E}$	Minimum ΔE	(kJ)	223.6
REX			
A_SPL	Noise parameter	(dB(A)/kW)	Confidential
B_SPL	Noise parameter	(dB(A))	Confidential
A_g	Generated power parameter	(1/kW)	Confidential
B_g	Generated power parameter	$(-)$	Confidential
C_g	Generated power parameter	(kW)	Confidential
$p_\mathrm{g}^{(1)}$	Generated power breakpoint	(kW)	20
$p_\mathrm{g}^{(2)}$	Generated power breakpoint	(kW)	25
λ_f	Diesel lower heating value	(MJ/kg)	42.5
$\overline{\vartheta}$	Coolant warmed-up temperature	(°C)	60
$\underline{\vartheta}$	Room temperature	(°C)	20
P_thr	Idling power threshold	(kW)	2
$\overline{P_\mathrm{g}}(\overline{\vartheta})$	Maximum power (warmed-up)	(kW)	35
$\overline{P_\mathrm{g}}(\underline{\vartheta})$	Maximum power (cold)	(kW)	27
$\underline{P_\mathrm{g}}$	Minimum power	(kW)	2
Price	Price	(k€)	10
Cost Function			
T_s	Sampling time	(s)	1
α_ϵ	Grid energy cost	$(€\ \mathrm{kW^{-1}\ h^{-1}})$	0.125
β_ϵ	Battery cost	$(€\ \mathrm{kW^{-1}\ h^{-1}})$	400
γ_ϵ	REX fuel cost	$(€\ \mathrm{kW^{-1}\ h^{-1}})$	0.104
$\delta_{\epsilon,0}$	REX noise cost (baseline)	$(€\ \mathrm{dB(A)^{-1}\ h^{-1}})$	0.018

model of (23)). This extends available results in the literature for linear difference equations (Damm et al. (2014)), and allows to employ the closed-loop performance and convergence results from Müller and Grüne (2016); Zanon et al. (2017); Faulwasser et al. (2018) also to systems described by nonlinear, convex difference inclusions.

In this work, the difference inclusions are formalized as follows:

$$\begin{aligned} x(k+1) \in F(x(k),u(k),r(k)) = \\ = \{y \in \mathbb{R}^\mathrm{n} | y \leq f(x(k),u(k),r(k))\}, \end{aligned} \tag{32}$$

where f is a concave and continuous function. Moreover, $x \in \mathbb{R}^\mathrm{n}$ denotes the state variables, $u \in \mathbb{R}^\mathrm{m}$ the control variables, and $r \in \mathbb{R}^\mathrm{w}$ the reference signals. Therefore, the feasible tuples (x,u,r) are collected in the following set, which is assumed to be compact:

$$\mathbb{Y} := \{(x,u,r) \in \mathbb{R}^\mathrm{n} \times \mathbb{R}^\mathrm{m} \times \mathbb{R}^\mathrm{w} | g_\mathrm{i}(x,u,r) \leq 0 \text{ for all } g_\mathrm{i} \in \mathscr{G}\} \tag{33}$$

with $\mathscr{G}$ the set of in total I constraints, and $g_\mathrm{i} : \mathbb{R}^\mathrm{n} \times \mathbb{R}^\mathrm{m} \times \mathbb{R}^\mathrm{w} \to \mathbb{R}$ convex for all $i = 1,\dots,I$. Hence, the following sets are defined:

$$\mathbb{X} := \{x \in \mathbb{R}^\mathrm{n} | \exists\ u \in \mathbb{R}^\mathrm{m} \text{ and } r \in \mathbb{R}^\mathrm{w} \text{ with } (x,u,r) \in \mathbb{Y}\}, \tag{34}$$

$$\mathbb{U} := \{u \in \mathbb{R}^\mathrm{m} | \exists\ x \in \mathbb{R}^\mathrm{n} \text{ and } r \in \mathbb{R}^\mathrm{w} \text{ with } (x,u,r) \in \mathbb{Y}\}. \tag{35}$$

Ultimately, the general convex optimal control problem reads as follows:

$$\begin{aligned} \underset{x(0),u(0),\dots,x(N)}{\text{minimize}} \quad & \sum_{k=0}^{N-1} l(x(k),u(k),r(k)) + V_\mathrm{f}(x(N)) \\ \text{subject to} \quad & x(k+1) \in F(x(k),u(k),r(k)) = \\ & \quad = \{y \in \mathbb{R}^\mathrm{n} | y \leq f(x(k),u(k),r(k))\} \\ & g_\mathrm{i}(x(k),u(k),r(k)) \leq 0,\ \forall g_\mathrm{i} \in \mathscr{G} \end{aligned} \tag{36}$$

with l being the continuous and convex stage cost and V_f a suitable convex and continuous terminal cost.

4.1. Steady-state analysis

Let us introduce $(x^\star,u^\star,\bar{r})$, the optimal steady-state (or equilibrium point) retrieved from the solution of the following convex program:

$$\begin{aligned} \underset{x,u}{\text{minimize}} \quad & l(x,u,\bar{r}) \\ \text{subject to} \quad & x \leq f(x,u,\bar{r}) \\ & g_\mathrm{i}(x,u,\bar{r}) \leq 0,\ \forall g_\mathrm{i} \in \mathscr{G} \end{aligned} \tag{37}$$

where $\bar{r}$ is a constant reference signal and g_i (a generic convex constraint in $\mathscr{G}$) and $x - f(x,u,\bar{r})$ are convex in $(x,u,\bar{r})$. The equilibrium tuple $(x^\star,u^\star,\bar{r})$, solution of (37), satisfies $l(x^\star,u^\star,\bar{r}) \leq l(\tilde{x}^\star,\tilde{u}^\star,\bar{r})$ for all other equilibrium tuples $(\tilde{x}^\star,\tilde{u}^\star,\bar{r}) \in \mathbb{Y}$.

Definition 4.1. *Let $(x^\star,u^\star,\bar{r}) \in \mathbb{Y}$ be an equilibrium point of* (32)*, with $\bar{r}$ a constant reference signal. The system* (32) *is dissipative with respect to the supply rate $s(x,u,\bar{r}) = l(x,u,\bar{r}) - l(x^\star,u^\star,\bar{r})$ if there exists a storage function $\lambda : \mathbb{X} \to \mathbb{R}$ bounded from below such that the inequality:*

$$\lambda(x^+) - \lambda(x) \leq s(x,u,\bar{r}) \tag{38}$$

holds for all $(x,u,\bar{r}) \in \mathbb{Y}$ and all $x^+ \in F(x,u,\bar{r})$ (with x^+ denoting the time difference). The system is strictly dissipative if there exists $\alpha \in \mathscr{K}_\infty$[3] such that the following holds for all $(x,u,\bar{r}) \in \mathbb{Y}$ and all $x^+ \in F(x,u,\bar{r})$:

$$\lambda(x^+) - \lambda(x) + \alpha(\| (x - x^\star, u - u^\star) \|) \leq s(x,u,\bar{r}). \tag{39}$$

Proposition 4.1. *Consider the optimal control problem* (36) *with dynamics* (32)*, strictly convex l, a constraint set defined as in* (33) *with g_i convex, and a constant reference signal $\bar{r}$. Assume* (37) *to satisfy Slater's condition, i.e., there exists $(\hat{x},\hat{u},\bar{r}) \in \mathbb{Y}$ such that:*

$$\begin{aligned} &\hat{x} - f(\hat{x},\hat{u},\bar{r}) < 0, \\ &g_\mathrm{i}(\hat{x},\hat{u},\bar{r}) < 0, \ \forall g_\mathrm{i} \in \mathscr{G}. \end{aligned} \tag{40}$$

Then, there exists a vector $\nu_\mathrm{f} \in \mathbb{R}^\mathrm{n}_+$ such that the system is strictly dissipative with respect to the supply rate $s(x,u,\bar{r}) = l(x,u,\bar{r}) - l(x^\star,u^\star,\bar{r})$ and with $\lambda(x) = \nu_\mathrm{f}^\mathrm{T} x$.

The proof of Proposition 4.1 follows the lines of Damm et al. (2014), where the same result was shown for linear discrete-time systems (difference equations). Here, the results are extended to the case of nonlinear convex difference inclusions.

Proof. The strict convexity of l, together with the convexity and compactness of the constraints, ensures that the optimization problem (37) has a global and unique optimum $(x^\star,u^\star,\bar{r})$. Therefore, the Lagrangian for program (37) is introduced:

$$\mathscr{L}(x,u,\bar{r}) := l(x,u,\bar{r}) + (\nu_\mathrm{g}^\mathrm{T}, \nu_\mathrm{f}^\mathrm{T}) \begin{pmatrix} g_1(x,u,\bar{r}) \\ \vdots \\ g_\mathrm{I}(x,u,\bar{r}) \\ x - f(x,u,\bar{r}) \end{pmatrix}. \tag{41}$$

The validity of the Slater's condition implies strong duality[4] (Boyd and Vandenberghe (2004)), *i.e.*, the existence of Lagrange multipliers ν_g and ν_f such that:

$$\begin{aligned} \nu_\mathrm{g} \geq 0, \ \nu_\mathrm{f} \geq 0 \text{ and} \\ \nu_\mathrm{g} = 0, \text{ if } g_\mathrm{i}(x^\star,u^\star,\bar{r}) < 0 \\ \nu_\mathrm{f} = 0, \text{ if } x^\star - f(x^\star,u^\star,\bar{r}) < 0, \end{aligned} \tag{42}$$

and such that the following inequality holds:

$$\mathscr{L}^\star(x^\star,u^\star,\bar{r}) \leq \mathscr{L}(x,u,\bar{r}), \quad \forall\, (x,u,\bar{r}) \neq (x^\star,u^\star,\bar{r}). \tag{43}$$

Moreover, (43) is satisfied with strict inequality for strictly convex functions (Boyd and Vandenberghe (2004)). Let us define $\widehat{L}$ as follows:

$$\widehat{L}(x,u,\bar{r}) := l(x,u,\bar{r}) - l(x^\star,u^\star,\bar{r}) + (\nu_\mathrm{g}^\mathrm{T}, \nu_\mathrm{f}^\mathrm{T}) \begin{pmatrix} g_1(x,u,\bar{r}) \\ \vdots \\ g_\mathrm{I}(x,u,\bar{r}) \\ x - f(x,u,\bar{r}) \end{pmatrix}. \tag{44}$$

Therefore, from (43) and (44):

$$\widehat{L}(x,u,\bar{r}) > (\nu_\mathrm{g}^\mathrm{T}, \nu_\mathrm{f}^\mathrm{T}) \begin{pmatrix} g_1(x^\star,u^\star,\bar{r}) \\ \vdots \\ g_\mathrm{I}(x^\star,u^\star,\bar{r}) \\ x^\star - f(x^\star,u^\star,\bar{r}) \end{pmatrix} = 0 \tag{45}$$

for all $(x,u,\bar{r}) \neq (x^\star,u^\star,\bar{r})$, due to the complementary slackness condition (42). Given that $\nu_\mathrm{g}^\mathrm{T}[g_1(x,u,\bar{r}) \dots g_\mathrm{I}(x,u,\bar{r})]^\mathrm{T} \leq 0$ for all $(x,u,\bar{r}) \in \mathbb{Y}$, $\widehat{L}$ is bounded from above on $\mathbb{Y}$ as follows:

$$L(x,u,\bar{r}) := l(x,u,\bar{r}) - l(x^\star,u^\star,\bar{r}) + \nu_\mathrm{f}^\mathrm{T}(x - f(x,u,\bar{r})) \geq \widehat{L}(x,u,\bar{r}). \tag{46}$$

Now consider any tuple $(x,u,\bar{r}) \in \mathbb{Y}$ together with x^+ satisfying the difference inclusion (32), *i.e.*,

$$x^+ \leq f(x,u,\bar{r}). \tag{47}$$

Since $\nu_\mathrm{f} \geq 0$, for any such points the following inequality must hold:

$$\begin{aligned} L'(x,u,\bar{r},x^+) := l(x,u,\bar{r}) - l(x^\star,u^\star,\bar{r}) + \nu_\mathrm{f}^\mathrm{T}(x - x^+) \geq \\ \geq L(x,u,\bar{r}) \geq \widehat{L}(x,u,\bar{r}). \end{aligned} \tag{48}$$

That is, if (47) holds with strict inequality, $\widehat{L}$ is strictly bounded from above by L'. Choosing the storage function $\lambda(x) = \nu_\mathrm{f}^\mathrm{T} x$, from (48) the desired strict dissipativity result follows if there exists some $\alpha \in \mathscr{K}_\infty$, such that the following inequality holds for all $(x,u,\bar{r}) \in \mathbb{Y}$ and for all x^+ satisfying (47):

$$L'(x,u,\bar{r},x^+) \geq \alpha(\| (x - x^\star, u - u^\star) \|). \tag{49}$$

Since $L'(x,u,\bar{r},x^+) > 0$ for all $(x,u,\bar{r}) \in \mathbb{Y}$ and x^+ satisfying (47) with $(x,u,\bar{r},x^+) \neq (x^\star,u^\star,\bar{r},x^\star)$ and $L'(x^\star,u^\star,\bar{r},x^\star) = 0$, Lemma A.1 of Berberich et al. (2020) can be applied to prove the validity of (49), thus ensuring strict dissipativity. □

4.2. P-periodic orbit

Dissipativity is now proven for a periodic reference signal $\mathbf{r}$ obtained concatenating multiple times the reference signal $\bar{\mathbf{r}} = [\bar{r}(1) \dots \bar{r}(k) \dots \bar{r}(P-1)]$. Given the compactness of $\mathbb{Y}$, a P-periodic solution $\mathscr{P} = \{(x(0),u(0),\bar{r}(0)), \dots, (x(P-1),u(P-1),\bar{r}(P-1))\}$, obtained solving the following optimal control problem over $\bar{\mathbf{r}}$, exists:

$$\begin{aligned} \underset{\substack{x(0),u(0),\\ \dots \\ x(P-1),u(P-1)}}{\text{minimize}} \quad & \sum_{k=0}^{P-1} l(x(k),u(k),\bar{r}(k)) \\ \text{subject to} \quad & x(k+1) \in F(x(k),u(k),\bar{r}(k)) = \\ & \quad = \{y \in \mathbb{R}^\mathrm{n} | y \leq f(x(k),u(k),\bar{r}(k))\}, \\ & k = 0, \dots, P-2 \\ & x(0) \in F(x(P-1),u(P-1),\bar{r}(P-1)) = \\ & \quad = \{y \in \mathbb{R}^\mathrm{n} | y \leq f(x(P-1),u(P-1),\bar{r}(P-1))\}, \\ & g_\mathrm{i}(x(k),u(k),r(k)) \leq 0, \text{ for } k = 0, \dots, P-1 \text{ and } \forall g_\mathrm{i} \in \mathscr{G} \end{aligned} \tag{50}$$

[3] $\mathscr{K}_\infty := \{\alpha \in \mathscr{K} | \alpha \text{ is unbounded}\}$ and
$\mathscr{K} := \{\alpha : \mathbb{R}_+ \to \mathbb{R}_+ | \alpha \text{ continuous, strictly increasing, } \alpha(0) = 0\}$.

[4] Strong duality means that the optimal solutions to the primal and dual problem are the same (Boyd and Vandenberghe (2004)).

Definition 4.2. *Let $\mathscr{P}^\star \subset \mathbb{Y}$ be a periodic orbit, solution of the problem* (50)*, with $\bar{\mathbf{r}}$ the reference signal. The system* (32) *is said to be P-periodic dissipative with respect to the supply rate $s(x,u,\bar{r}(k)) = l(x,u,\bar{r}(k)) - l(x^\star(k),u^\star(k),\bar{r}(k))$ if there exist storage functions $\lambda_\mathrm{k} : \mathbb{X} \to \mathbb{R}$ bounded from below (for $k = 0,\dots,P-1$) such that the inequality:*

$$\lambda_{\mathrm{k}+1}\left(x^+\right) - \lambda_\mathrm{k}\left(x\right) \leq s(x,u,\bar{r}(k)) \tag{51}$$

holds for all $(x,u,\bar{r}(k)) \in \mathbb{Y}$ and all $x^+ \in F(x,u,\bar{r}(k))$, with $k = 0,\dots,P-1$. The system is P-periodic strictly dissipative if there exists $\alpha \in \mathscr{K}_\infty$ such that the following holds for all $(x,u,\bar{r}(k)) \in \mathbb{Y}$ and all $x^+ \in F(x,u,\bar{r}(k))$:

$$\lambda_{\mathrm{k}+1}\left(x^+\right) - \lambda_\mathrm{k}\left(x\right) + \alpha(\parallel (x,u) \parallel_\Pi) \leq s(x,u,\bar{r}(k)) \tag{52}$$

with $k = 0,\dots,P-1$ and $\Pi = \{(x^\star(0),u^\star(0)),\dots,(x^\star(P-1), u^\star(P-1))\}$ containing the elements of $\mathscr{P}^\star$.

According to Köhler et al. (2018), in (52) the term $\parallel (x,u) \parallel_\Pi$ denotes the distance to the orbit, *i.e.*,

$$\parallel (x,u) \parallel_\Pi = \min_{k\in\{0,\dots,P-1\}} \parallel x - x^\star(k) \parallel + \parallel u - u^\star(k) \parallel . \tag{53}$$

Proposition 4.2. *Consider the periodic optimal control problem* (50) *with dynamics* (32)*, strictly convex l, a constraint set defined as in* (33) *with g_i convex, and a periodic reference signal* $\mathbf{r}$*. Assuming Slater's condition to be satisfied, there exist storage functions $\lambda_\mathrm{k}(x)$ such that system* (32) *is P-periodic strictly dissipative with respect to the supply rate $s(x,u,\bar{r}(k)) = l(x,u,\bar{r}(k)) - l(x^\star(k),u^\star(k),\bar{r}(k))$.*

Most of the concepts introduced in the proof of Proposition 4.1 apply also for Proposition 4.2.

Proof. The strict convexity of l, together with convexity and compactness of the constraints, ensures that the optimization problem (50) has a global and unique optimal periodic orbit $\mathscr{P}^\star$. Therefore, the Lagrangian for program (50) reads as follows:

$$\begin{aligned}\mathscr{L}(\mathscr{P}) \coloneqq & \sum_{k=0}^{P-1} l\big(x(k),u(k),\bar{r}(k)\big) + \\ & \sum_{k=0}^{P-2} \nu_{\mathrm{f,k}+1}^{\mathrm{T}}\big(x(k+1) - f(x(k),u(k),\bar{r}(k))\big) + \\ & \nu_{\mathrm{f},0}^{\mathrm{T}}\big(x(0) - f(x(P-1),u(P-1),\bar{r}(P-1))\big) + \\ & \sum_{k=0}^{P-1} \nu_{\mathrm{g,k}}^{\mathrm{T}} g\big(x(k),u(k),\bar{r}(k)\big).\end{aligned} \tag{54}$$

To improve readability, it is assumed that $g = [g_1 \dots g_\mathrm{I}]^\mathrm{T}$. Thus, the validity of the Slater's condition implies strong duality (Boyd and Vandenberghe (2004)), *i.e.*, the existence of Lagrange multipliers $\nu_{\mathrm{g,k}}$ and $\nu_{\mathrm{f,k}}$ such that:

$$\begin{aligned}\nu_{\mathrm{g,k}} \geq 0,\ \nu_{\mathrm{f,k}} \geq 0 \text{ and} \\ \nu_{\mathrm{g,k}} = 0,\ \text{if } g_\mathrm{i}(x^\star(k),u^\star(k),\bar{r}(k)) < 0 \\ \nu_{\mathrm{f,k}} = 0,\ \text{if } x^\star(k) - f(x^\star(k-1),u^\star(k-1),\bar{r}(k-1)) < 0,\end{aligned} \tag{55}$$

and such that the following inequality holds:

$$\mathscr{L}^\star(\mathscr{P}^\star) \leq \mathscr{L}(\mathscr{P}) \tag{56}$$

for all trajectories $\mathscr{P}$ of length P (not necessary periodic). Moreover, for all such $\mathscr{P}$ with $\mathscr{P} \neq \mathscr{P}^\star$, (56) is satisfied with strict inequality for strictly convex functions. Let us define the $\widehat{L}$ as follows:

$$\begin{aligned}\widehat{L}(\mathscr{P}) \coloneqq & \sum_{k=0}^{P-1} \big[l\big(x(k),u(k),\bar{r}(k)\big) - l\big(x^\star(k),u^\star(k),\bar{r}(k)\big)\big] + \\ & \sum_{k=0}^{P-2} \nu_{\mathrm{f,k}+1}^{\mathrm{T}}\big(x(k+1) - f(x(k),u(k),\bar{r}(k))\big) + \\ & \nu_{\mathrm{f},0}^{\mathrm{T}}\big(x(0) - f(x(P-1),u(P-1),\bar{r}(P-1))\big) + \\ & \sum_{k=0}^{P-1} \nu_{\mathrm{g,k}}^{\mathrm{T}} g\big(x(k),u(k),\bar{r}(k)\big).\end{aligned} \tag{57}$$

Therefore, from (56) and (57):

$$\begin{aligned}\widehat{L}(\mathscr{P}) > & \sum_{k=0}^{P-2} \nu_{\mathrm{f,k}+1}^{\mathrm{T}}\big(x^\star(k+1) - f(x^\star(k),u^\star(k),\bar{r}(k))\big) + \\ & \nu_{\mathrm{f},0}^{\mathrm{T}}\big(x^\star(0) - f(x^\star(P-1),u^\star(P-1),\bar{r}(P-1))\big) + \\ & \sum_{k=0}^{P-1} \nu_{\mathrm{g,k}}^{\mathrm{T}} g\big(x^\star(k),u^\star(k),\bar{r}(k)\big) = 0\end{aligned} \tag{58}$$

for all $\mathscr{P} \neq \mathscr{P}^\star$, due to the complementary slackness condition (55). Given that $\sum_{k=0}^{P-1} \nu_{\mathrm{g,k}}^{\mathrm{T}} g\big(x(k),u(k),\bar{r}(k)\big) \leq 0$, $\widehat{L}$ is bounded from above on $\mathbb{Y}$ as follows:

$$\begin{aligned}L(\mathscr{P}) \coloneqq & \sum_{k=0}^{P-1} \big[l\big(x(k),u(k),\bar{r}(k)\big) - l\big(x^\star(k),u^\star(k),\bar{r}(k)\big)\big] + \\ & \sum_{k=0}^{P-2} \nu_{\mathrm{f,k}+1}^{\mathrm{T}}\big(x(k+1) - f(x(k),u(k),\bar{r}(k))\big) + \\ & \nu_{\mathrm{f},0}^{\mathrm{T}}\big(x(0) - f(x(P-1),u(P-1),\bar{r}(P-1))\big) \geq \widehat{L}(\mathscr{P}).\end{aligned} \tag{59}$$

Since $\nu_{\mathrm{f,k}} \geq 0$, for all the feasible trajectories $\mathscr{P}$ of the difference inclusion, such that $\mathscr{P}$ is not equal to $\mathscr{P}^\star$, the following holds:

$$\begin{aligned}L'(\mathscr{P}) \coloneqq & \sum_{k=0}^{P-1} \big[l(x(k),u(k),\bar{r}(k)) - l(x^\star(k),u^\star(k),\bar{r}(k))\big] + \\ & \nu_{\mathrm{f},0}^{\mathrm{T}}\big(x(0) - f(x(P-1),u(P-1),\bar{r}(P-1))\big) \geq L(\mathscr{P}) > 0\end{aligned} \tag{60}$$

with $L'(\mathscr{P}) = 0$ only along the optimal periodic orbit $\mathscr{P}^\star$. Therefore, relying on Lemma A.1 of Berberich et al. (2020) allows to conclude that the left hand side of (60) is greater than or equal to a function α, *i.e.*,

$$L'(\mathscr{P}) \geq \alpha\left(\sum_{k=0}^{P-1} \parallel (x(k),u(k)) \parallel_\Pi\right) \geq \frac{1}{P}\sum_{k=0}^{P-1} \alpha(||(x(k),u(k))||_\Pi). \tag{61}$$

Considering a storage function $\lambda(x) = v_{f,0}^{T} x$ and an average cost $l_p = \frac{1}{P}\sum_{k=0}^{P-1} l(x^\star(k), u^\star(k), \bar{r}(k))$, (61) is equivalent to Assumption 2 of Köhler et al. (2018). Eventually, Proposition 1 of Köhler et al. (2018) can be used to conclude that (61) is equivalent to the existence of storage functions $\lambda_k(x)$ such that (52) holds. □

4.3. EMPC formulation

Starting from (36), the convex MPC problem is formulated as follows:

$$\begin{aligned} \underset{x(0),u(0),\dots,x(N_p)}{\text{minimize}} \quad & \sum_{\tau=0}^{N_p-1} l\left(x(k+\tau|k), u(k+\tau|k), r(k+\tau|k)\right) + V_f(x(N_p|k)) \\ \text{subject to} \quad & x(k+\tau+1|k) \in F\left(x(k+\tau|k), u(k+\tau|k), r(k+\tau|k)\right) = \\ & = \{y \in \mathbb{R}^n | y \le f\left(x(k+\tau|k), u(k+\tau|k), r(k+\tau|k)\right)\} \\ & g_i(x(k+\tau|k), u(k+\tau|k), r(k+\tau|k)) \le 0, \ \forall g_i \in \mathscr{G} \end{aligned} \tag{62}$$

for $\tau = 0, \dots, N_p - 1$ and $N_p \le N$ the prediction horizon. Therefore, at each time instant k, the optimal control problem is solved on the horizon N_p. Then, the *receding horizon* principle is applied and only the first control variable is applied for a duration equal to T_s.

5. Results for the Energy Management Problem

In this section, the validity of the dissipativity conditions (proved in Section 4) and their implications are shown for the EMS problem at hand. To establish a direct correspondence with the previous section, the following definitions are introduced:

- $x := \Delta E$ is the state variable;
- $u := [P_g^{(1)} \ P_g^{(2)} \ P_g^{(3)} \ P_b]^T$ are the control inputs;
- $r := P_{ec}$ is the reference signal.

In this scenario, the stage cost $l : \mathbb{Y} \to \mathbb{R}$ is characterized by the following structure:

$$\begin{aligned} l(x(k), u(k), r(k)) &= l_1(x(k)) + l_2(u(k), r(k)) = \\ &= -\xi x(k) + l_2(u(k), r(k)) \end{aligned} \tag{63}$$

with l_1 and l_2 defined as in (24) and $\xi = \frac{\alpha_\epsilon}{\eta_{grid}} \in \mathbb{R}_+ \backslash \{0\}$ a user defined parameter. Given (63), the minimum cost is always obtained when the following condition is met:

$$x(k+1) \in F(x,u,r) = \{y \in \mathbb{R} | y = f\left(x(k), u(k), r(k)\right)\} \tag{64}$$

i.e., along the boundary of the *hypograph*. As a matter of fact, if $f\left(x(k), u(k), r(k)\right)$ is positive, $l_1(x(k+1)) < 0$ and its minimum is obtained when $x(k+1) = f(x(k), u(k), r(k))$. Similarly, if $f\left(x(k), u(k), r(k)\right)$ is negative, $l_1(x(k+1)) > 0$ and its minimum is obtained again for $x(k+1) = f(x(k), u(k), r(k))$.

Therefore, the MPC is formalized as in (62). As shown by (18), the REX delivered power is limited to $\overline{P_g}(\underline{\vartheta})$ just during the first 6 (min) of operation, *i.e.*, the time needed to warm-up the ICE. In the MPC framework, this behavior is ensured relying on two complementary formulations of (62). In practice, the former is embedding the constraint with $\overline{P_g}(\underline{\vartheta})$, useful for the warming-up transient. Conversely, the latter is describing the normal REX operation, *i.e.*, the warmed-up scenario with a maximum delivered power $\overline{P_g}(\overline{\vartheta})$.

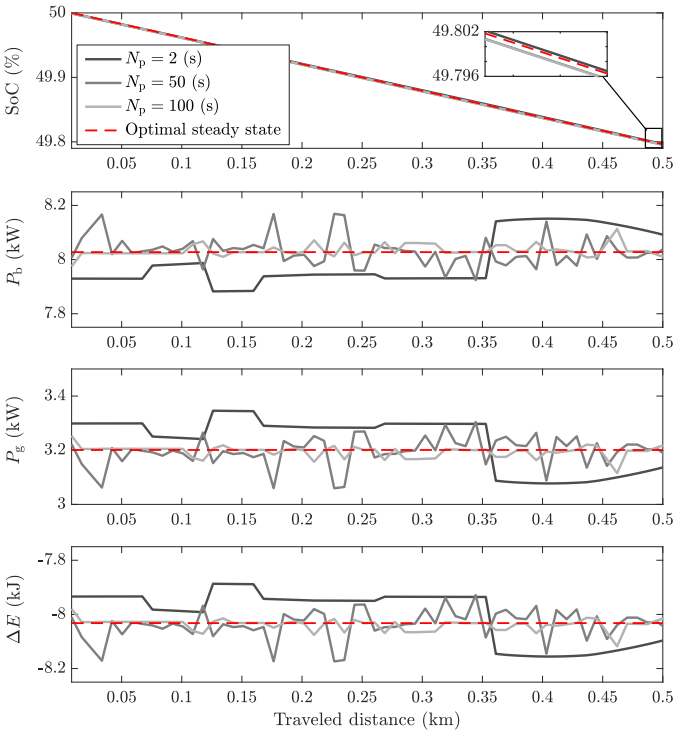

Figure 6: Solution of the MPC problem (62) for different values of the prediction horizon N_p, considering a constant vehicle speed of 30 (km/h) and a SoC initial condition of 50%. Clearly, increasing N_p, the MPC solution approaches the optimal steady-state. To ease readers' comprehension, solutions are zoomed between 0 and 500 (m). The MPC prediction is obtained assuming perfect knowledge of the future driving cycle.

In the remainder of the section, the MPC problem (62) is solved. The convergence of the online solutions to the optimal steady-state and to the optimal P-periodic solution is analyzed. Finally, some results on a real world driving condition are shown.

5.1. Steady-state

Assuming the REX to be warmed-up and considering a constant speed profile at 30 (km/h) (and thus a constant power request of $\bar{r} = 11.23$ (kW) – the vehicle is assumed to be already at the target speed and the acceleration transient is neglected –), the optimal steady-state is computed solving (37), leading to:

$$P_b^\star = 8.03 \text{ (kW)}, \ P_g^\star = 3.20 \text{ (kW)} \ [5], \ \Delta E^\star = -8.03 \text{ (kJ)}. \tag{65}$$

Therefore, the system (23) is proven to be dissipative with respect to the optimal steady-state (65) checking whether (38) is

[5] $P_g^\star$ is given by (31).

	Offline	MPC		
N_p (s)	NA	2	50	100
SoC (%)	45.8269	45.9113	45.8192	45.8226
J (€)	1.7589	1.7600	1.7599	1.7599
J_e (€)	0.3634	0.3560	0.3640	0.3637
J_a (€)	0.2539	0.2488	0.2544	0.2542
J_f (€)	0.5337	0.5464	0.5331	0.5336
J_n (€)	0.6079	0.6087	0.6084	0.6084
Opt. time	71.6 (s)	0.008 (s/step)	0.036 (s/step)	0.098 (s/step)

* NA: Not Applicable

Table 2: Sensitivity analysis with respect to the prediction horizon N_p for the steady-state scenario. With increasing N_p, the average computation time to solve the optimization problem increases (but is always below the sampling time of $T_s = 1$ (s)). MPC results are compared to the optimal steady-state solution applied over a traveled distance of 10 (km). Moreover, the MPC prediction is obtained assuming perfect knowledge of the future driving cycle.

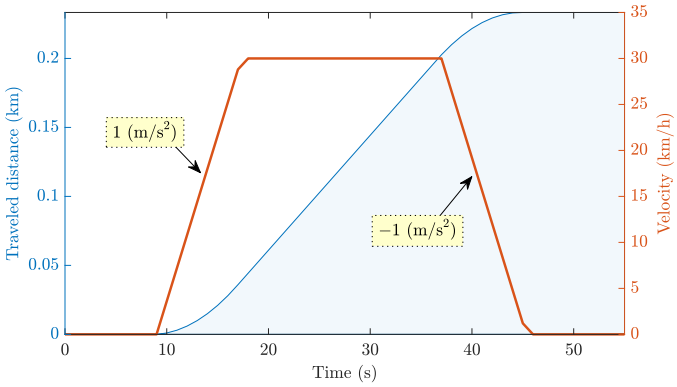

Figure 7: Trapezoidal driving cycle. The area plot denotes the traveled distance.

satisfied for each tuple $(x,u,\bar{r}) \in \mathbb{Y}$. In practice, for the EMS problem at hand, (38) is rewritten as follows:

$$\nu_f(f(x,u,\bar{r}) - x) \leq l(x,u,\bar{r}) - l(x^\star,u^\star,\bar{r}). \tag{66}$$

For $\nu_f = 0.038$ (€/MJ) (retrieved from the solution of the dual problem of (37)), the dissipativity condition holds true. Thus, for a long enough prediction horizon, the solution of the EMPC without terminal constraints defined as in (62) is expected to converge to a neighborhood of the optimal steady-state (65) (Faulwasser et al. (2018)). This is numerically proved solving (62) over a traveled distance of 10 (km) while assuming a constant vehicle speed of 30 (km/h). As shown by Figure 6, while increasing N_p the MPC approaches the optimal steady-state at the cost of increasing the average optimization step time (as shown by the last row of Table 2). In this scenario, the MPC prediction is obtained assuming perfect knowledge of the future driving cycle.

5.2. *P-periodic solution*

Analogously to the steady-state scenario, the REX is assumed to be warmed-up. Thus, the optimal P-periodic orbit is obtained solving (50) offline[6] with a periodic reference $\mathbf{r}$.

[6]Offline solution: computed from (24) over the horizon N assuming a perfect knowledge of the driving cycle.

	Offline	MPC		
N_p (s)	NA	2	50	100
SoC (%)	44.7373	44.9212	44.7667	44.7792
J (€)	8.014	8.020	8.019	8.019
J_e (€)	0.4581	0.4421	0.4556	0.4545
J_a (€)	1.1690	1.1578	1.1672	1.1664
J_f (€)	0.8283	0.8551	0.8327	0.8345
J_n (€)	5.5586	5.5646	5.5636	5.5637
Opt. time	101.5 (s)	0.007 (s/step)	0.030 (s/step)	0.060 (s/step)

* NA: Not Applicable

Table 3: Sensitivity analysis with respect to the prediction horizon N_p for the P-periodic scenario. With increasing N_p, the average computation time to solve the optimization problem increases (but is always below the sampling time of $T_s = 1$ (s)). MPC results are compared to the optimal P-periodic solution obtained considering a traveled distance of 10 (km) (obtained concatenating the driving cycle of Figure 7). Moreover, the MPC prediction is obtained assuming perfect knowledge of the future driving cycle.

To this end, the trapezoidal speed profile of Figure 7 is considered and concatenated multiple times till a traveled distance of 10 (km) is reached. The concatenations lead to a periodic power request. Therefore, dissipativity is proven considering the solution over one period (as highlighted in Figure 8). Recalling Definition 4.2 and considering the special case of linear storage functions, for each k, the following condition must be satisfied:

$$\nu_{f,k+1} f(x,u,\bar{r}(k)) - \nu_{f,k} x \leq l(x,u,\bar{r}(k)) - l(x^\star(k),u^\star(k),\bar{r}(k)). \tag{67}$$

Using the Lagrange multiplier trajectory of Figure 9, one can conclude from Proposition 4.2 that there exist storage functions λ_k such that periodic dissipativity as specified in Definition 4.2 holds. Numerical simulations over a traveled distance of 10 (km) (considering several concatenations of the speed profile in Figure 7) show the convergence of the EMPC scheme to a neighborhood of the optimal periodic orbit. Since periodic dissipativity holds, this means that the closed-loop system exhibits approximately optimal performance (converges to a neighborhood of the optimal periodic orbit, which by dissipativity is the optimal system behavior). Note that for implementing the EMPC scheme, the optimal P-periodic orbit does not have to be known, but just for verifying periodic dissipativity. As shown by Figure 8, while increasing N_p the MPC approaches the optimal periodic solution at the cost of increasing the average optimization step time (as shown by Table 3).

5.3. *Real-world driving cycle*

The real-world driving cycle is generated according to Appendix A over a traveled distance of 20 (km). The MPC solutions are computed considering different prediction horizons N_p and assuming a perfect knowledge of the driving cycle. Even in this complex scenario, numerical simulations show the MPC scheme to converge to the optimal offline benchmark, computed solving (24) (see Figure 10). As shown by Table 4, even the

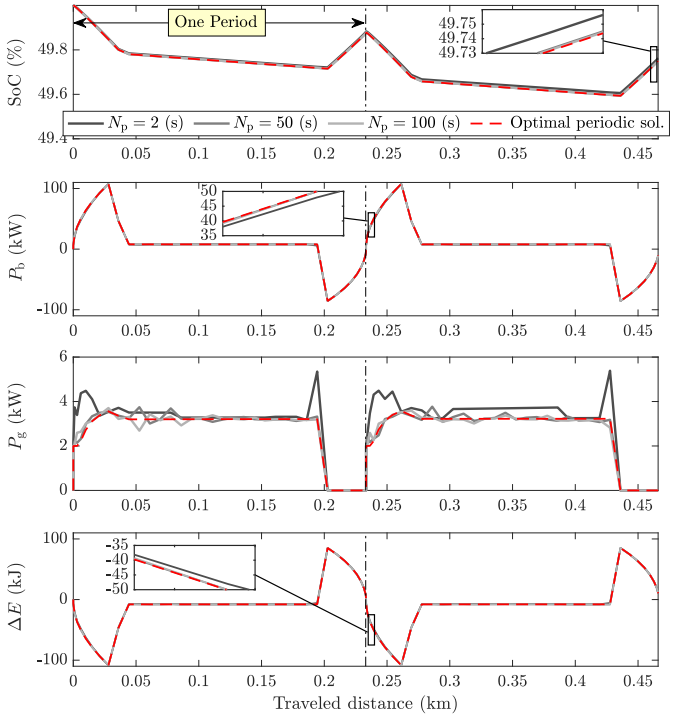

Figure 8: Solution of the MPC problem (62) for different values of the prediction horizon N_p, considering several concatenations of the driving cycle of Figure 7 and a SoC initial condition equal to 50%. Clearly, increasing N_p, the MPC solution converges to the optimal P-periodic solution. To ease readers' comprehension, solutions are zoomed between 0 and 450 (m).

shortest prediction window allows for a satisfactory approximation of the offline solution, leading to a final cost difference of 0.01 (€). Eventually, Figure 11 shows the validity of the EMPC convergence results even for a parameters setup favoring the REX usage, *i.e.*, for $N_b = 3000$ $(-)$ and $\gamma_\epsilon = 0.074$ $(€kW^{-1}h^{-1})$ [7]. In this scenario, the EMPC solution and the optimal benchmark are close for both cold and warmed-up engine operation. It is worth to mention that also other cost configurations can be used within the EMPC setup. For example, a lower baseline noise cost $\delta_{\epsilon,0}$ will generally result in a higher usage of the REX and vice versa.

In this work, a perfect knowledge of the driving style is assumed. Clearly, since the driving cycle is usually not known a priori, other prediction strategies can be adopted. For instance, the driving cycle can be assumed constant over the prediction horizon or, as shown by Corno and Pozzato (2019), a Markov chain based driver's behavior learning mechanism in connection with robust/stochastic MPC schemes (Bayer et al. (2016)) may be introduced (in order to ensure robustness with respect to modifications of the driving style). Since this is out of the scope of this work, the introduction of different prediction strategies, together with the analysis of the effectiveness of the proposed MPC on a (more realistic) forward powertrain modeling, is left for future developments.

[7] Typical U.S.A. diesel price.

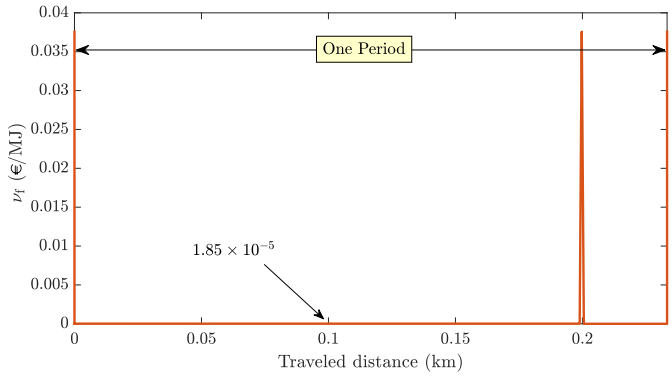

Figure 9: Trajectory of the Lagrange multiplier over one period. The trajectory is the one satisfying (67) while minimizing the following ℓ^2 norm: $\sqrt{\sum_k |\nu_{f,k}|^2}$.

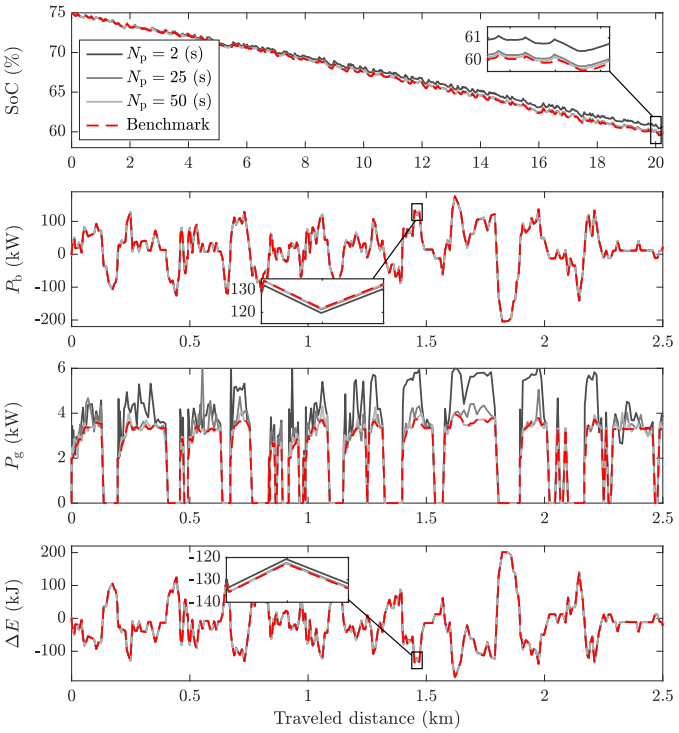

Figure 10: Real-world scenario. The optimal control problem is solved over a traveled distance of 20 (km) for different prediction horizons N_p. Exception given for the battery state of charge, the solutions are zoomed between 0 and 2.5 (km).

6. Conclusions

In this paper, the problem of online energy management for hybrid electric vehicles is addressed. Defining a *least costly* objective function, the online solution is obtained relying on the EMPC framework. Dissipativity properties for steady-state and periodic operation of the system at hand are proved. Therefore, some guarantees for the convergence of the economic model predictive control to the optimum are provided. Given the close to optimum performance of the proposed EMPC, the strategy outlined in the paper is useful not only for on board energy management but also for powertrain sizing issues or sensitivity analysis. As a matter of fact, it allows to solve the energy man-

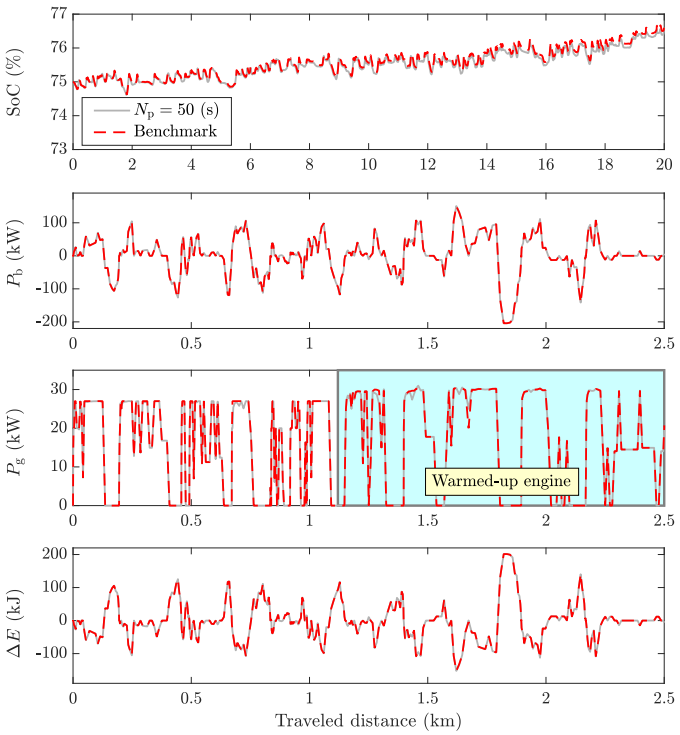

Figure 11: Real-world scenario for $N_b = 3000$ $(-)$ and $\gamma_{€} = 0.074$ $(€kW^{-1}h^{-1})$. The optimal control problem is solved over a traveled distance of 20 (km) for $N_p = 50$ (s). The behavior for cold and warmed-up engine is shown. Exception given for the battery state of charge, the solutions are zoomed between 0 and 2.5 (km).

	Offline	**MPC**		
N_p (s)	NA	2	25	50
SoC (%)	59.8913	60.7559	60.0751	59.9730
J (€)	17.8830	17.8863	17.8835	17.8832
J_e (€)	1.3272	1.2515	1.3111	1.3200
J_a (€)	3.9395	3.887	3.9283	3.9345
J_f (€)	1.5416	1.6683	1.5682	1.5533
J_n (€)	11.0747	11.0795	11.0759	11.0753
Opt. time	330.0 (s)	0.008 (s/step)	0.022 (s/step)	0.040 (s/step)

* NA: Not Applicable

Table 4: Sensitivity analysis with respect to the prediction horizon N_p for the real-world scenario. With increasing N_p, the average computation time to solve the optimization problem increases (but is always below the sampling time of $T_s = 1$ (s)). MPC solutions are compared to the offline benchmark policy computed over a traveled distance of 20 (km). Moreover, the MPC prediction is obtained assuming perfect knowledge of the future driving cycle.

agement problem with a reasonable computational effort even over long horizons. This is usually a hard task if the solution of (24) is carried out in a non-causal fashion over the complete horizon N. As a matter of fact, mixed integer convex problems, even though with a convex feasible set (when integrality constraints are relaxed), are NP-hard (Bonami et al. (2012)). In this work, a simple idling heuristic based on a power threshold P_{thr} is also defined. Nothing prevents from defining more complex rules to manage the engine idling behavior. As a matter of fact, convergence results would still apply.

Future works will investigate the possibility of introducing complex models, *i.e.*, without approximations and relaxations, to describe more accurately the powertrain behavior in the simulations. Moreover, on board implementation of the proposed EMPC solution of the EMS problem will be analyzed. Results will be compared to state of the art online strategies such as rule-based controllers (Jalil et al. (1997); Lin et al. (2001); Banvait et al. (2009)) and the equivalent consumption minimization strategy (Musardo et al. (2005); Pisu and Rizzoni (2007)).

Acknowledgement

This work was partially sponsored by Steyr Motors GmbH and the Linz Center of Mechatronics (LCM).

Appendix A. Driving cycle generation

This section aims to harmonize the driving cycle generation mechanism for public buses. Conversely to automobiles, buses are characterized by the presence of stops along the trip and by the loading/unloading of passengers, which considerably varies the mass of the vehicle. Therefore, being able to generate informative driving cycles is of paramount importance in order to characterize the energy behavior of the vehicle in different scenarios.

To this aim, the driving cycle is generated considering circular routes, *i.e.*, bus routes with coincident starting point and end of line. A generic route is denoted by ρ and it is characterized by a traveled distance of d kilometers. Stops are randomly chosen along the trip (on a distance base) in order to satisfy the following properties:

- A stop is characterized by at least 15 (s) of zero vehicle speed;
- Stops are separated at least by 2 (km).

Passengers' loading/unloading may occur only during bus stops, with the average passenger's weight m_{psg} being 70 (kg) (Walpole et al. (2012)). The speed profile between two stops is randomly generated relying on a Markov chain stochastic process with states $\mathscr{W} = \{\mathbf{w}_1, \mathbf{w}_2, \dots, \mathbf{w}_s\} \subseteq \mathbb{R}^2$, where s is the number of states. According to Lee et al. (2011), each state $\mathbf{w}_{\hat{m}}$, for all $\hat{m} \in \{1,2,\dots,s\}$, is defined as a couple $(v_{\hat{m}}, a_{\hat{m}})$ with the scalar quantities $v_{\hat{m}}$ and $a_{\hat{m}}$ denoting speed and acceleration, respectively. Therefore, the driving cycle is parametrized as transitions from a (velocity,acceleration) pair to another. All the probabilities of transitioning, in one time step, from any state to any other state are summarized in the transition probability matrix $\mathscr{T} \in \mathbb{R}^{s \times s}$:

$$\mathscr{T}_{\hat{m}\hat{n}} = \Pr\big(\mathbf{w}(k+1) = \mathbf{w}_{\hat{n}} | \mathbf{w}(k) = \mathbf{w}_{\hat{m}}\big) = p_{\hat{m}\hat{n}} \qquad \text{(A.1)}$$

for all $\hat{n}, \hat{m} \in \{1,2,\dots,s\}$. Therefore, starting from the known driving cycle of Figure A.12, the transition probability matrix

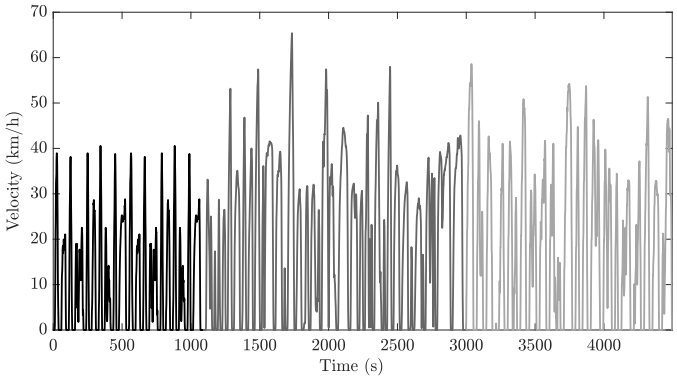

Figure A.12: Driving cycle used to train the transition probability matrix for the Markov chain model. Shades of gray from dark to light denote the bus driving cycles in Manhattan (Kelly et al. (2016)), Orange County (Kelly et al. (2016)), and Graz (Austria), respectively. Road slope is zero over the whole driving cycle.

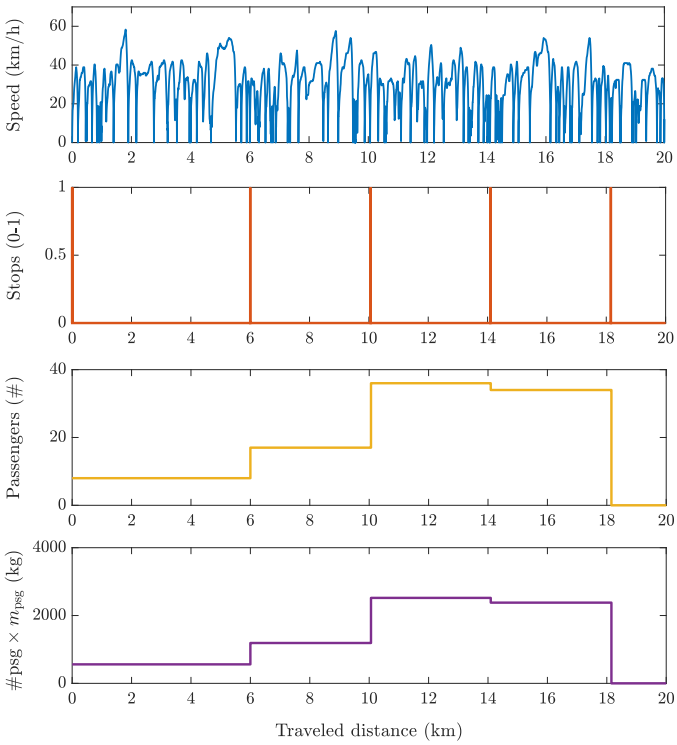

Figure A.13: Generated driving cycle over a traveled horizon of $d = 20$ (km). Stops are modeled as binary variables equal to one when a stop occurs.

is built computing the probability to move from a certain (velocity,acceleration) state $\hat{m}$ to another one $\hat{n}$ according to the following formula:

$$p_{\hat{m}\hat{n}} = \frac{\mathscr{N}_{\hat{m}\hat{n}}}{\sum_{j \in \mathscr{J}} \mathscr{N}_{\hat{m}j}} \tag{A.2}$$

where $\mathscr{N}_{\hat{m}j}$ is the number of times a transition occurs from state $\hat{m}$ to state j, and $\mathscr{J}$ is the set of reachable states from state $\hat{m}$. Figure A.13 shows an illustrative driving cycle generated with the aforementioned strategy. Considering a traveled distance of $d = 20$ (km), five stops are randomly located along the trip. Then, the speed profile between the stops is generated. Moreover, the number of passengers #psg is varied in correspondence of each bus stop. The overall mass variation due to loading and unloading of passengers is given by the product between #psg and m_{psg}. Clearly, the proposed approach can be used to generate driving cycles with higher traveled distances and different number of bus stops.

References

Banvait, H., Anwar, S., Chen, Y., 2009. A rule-based energy management strategy for plug-in hybrid electric vehicle (PHEV), in: American Control Conference, 2009. ACC'09., IEEE. pp. 3938–3943.

Bayer, F.A., Lorenzen, M., Müller, M.A., Allgöwer, F., 2016. Robust economic model predictive control using stochastic information. Automatica 74, 151–161.

Berberich, J., Köhler, J., Allgöwer, F., Müller, M.A., 2020. Dissipativity properties in constrained optimal control: a computational approach. Automatica 114, 108840.

Bonami, P., Kilinç, M., Linderoth, J., 2012. Algorithms and software for convex mixed integer nonlinear programs, in: Mixed integer nonlinear programming. Springer, pp. 1–39.

Boyd, S., Vandenberghe, L., 2004. Convex optimization. Cambridge university press.

Brogliato, B., Lozano, R., Maschke, B., Egeland, O., 2007. Dissipative systems analysis and control. Theory and Applications 2.

Corno, M., Pozzato, G., 2019. Active adaptive battery aging management for electric vehicles. IEEE Transactions on Vehicular Technology 69, 258–269.

Cory, W., 2010. Relationship between sound pressure and sound power levels. 2010 Eurovent. WG 1.

Damm, T., Gruüne, L., Stieler, M., Worthmann, K., 2014. An exponential turnpike theorem for dissipative discrete time optimal control problems. SIAM Journal on Control and Optimization 52, 1935–1957.

Elbert, P., Nüesch, T., Ritter, A., Murgovski, N., Guzzella, L., 2014. Engine on/off control for the energy management of a serial hybrid electric bus via convex optimization. IEEE Transactions on Vehicular Technology 63, 3549–3559.

Faulwasser, T., Grüne, L., Müller, M.A., et al., 2018. Economic nonlinear model predictive control. Foundations and Trends® in Systems and Control 5, 1–98.

Guanetti, J., Formentin, S., Savaresi, S.M., 2016. Energy management system for an electric vehicle with a rental range extender: A least costly approach. IEEE Transactions on Intelligent Transportation Systems 17, 3022–3034.

Guzzella, L., Sciarretta, A., et al., 2007. Vehicle propulsion systems. volume 1. Springer.

Helmers, E., Marx, P., 2012. Electric cars: technical characteristics and environmental impacts. Environmental Sciences Europe 24, 14.

Hu, X., Murgovski, N., Johannesson, L., Egardt, B., 2013. Energy efficiency analysis of a series plug-in hybrid electric bus with different energy management strategies and battery sizes. Applied Energy 111, 1001–1009.

Hu, X., Murgovski, N., Johannesson, L.M., Egardt, B., 2015. Optimal dimensioning and power management of a fuel cell/battery hybrid bus via convex programming. IEEE/ASME transactions on mechatronics 20, 457–468.

Jalil, N., Kheir, N.A., Salman, M., 1997. A rule-based energy management strategy for a series hybrid vehicle, in: American Control Conference, 1997. Proceedings of the 1997, IEEE. pp. 689–693.

Kelly, K., Prohaska, R., Ragatz, A., Konan, A., 2016. NREL driveCAT-chassis dynamometer test cycles.

Köhler, J., Müller, M.A., Allgöwer, F., 2018. On periodic dissipativity notions in economic model predictive control. IEEE Control Systems Letters 2, 501–506.

Lee, T.K., Adornato, B., Filipi, Z.S., 2011. Synthesis of real-world driving cycles and their use for estimating PHEV energy consumption and charging opportunities: Case study for midwest/us. IEEE Transactions on vehicular technology 60, 4153–4163.

Lin, C., Kang, J., Grizzle, J., Peng, H., 2001. Energy management strategy for a parallel hybrid electric truck, in: American Control Conference, 2001. Proceedings of the 2001, IEEE. pp. 2878–2883.

Müller, M.A., Grüne, L., 2016. Economic model predictive control without terminal constraints for optimal periodic behavior. Automatica 70, 128–139.

Müller, M.A., Grüne, L., Allgöwer, F., 2015. On the role of dissipativity in economic model predictive control. IFAC-PapersOnLine 48, 110–116.

Murgovski, N., Johannesson, L., Hellgren, J., Egardt, B., Sjöberg, J., 2011. Convex optimization of charging infrastructure design and component sizing of a plug-in series HEV powertrain. IFAC Proceedings Volumes 44, 13052–13057.

Murgovski, N., Johannesson, L., Sjöberg, J., 2012a. Convex modeling of energy buffers in power control applications. IFAC Proceedings Volumes 45, 92–99.

Murgovski, N., Johannesson, L., Sjöberg, J., Egardt, B., 2012b. Component sizing of a plug-in hybrid electric powertrain via convex optimization. Mechatronics 22, 106–120.

Musardo, C., Rizzoni, G., Guezennec, Y., Staccia, B., 2005. A-ECMS: An adaptive algorithm for hybrid electric vehicle energy management. European Journal of Control 11, 509–524.

Onori, S., Serrao, L., Rizzoni, G., 2016. Hybrid electric vehicles: Energy management strategies. Springer.

Pérez, L.V., Bossio, G.R., Moitre, D., García, G.O., 2006. Optimization of power management in an hybrid electric vehicle using dynamic programming. Mathematics and Computers in Simulation 73, 244–254.

Pisu, P., Rizzoni, G., 2007. A comparative study of supervisory control strategies for hybrid electric vehicles. IEEE Transactions on Control Systems Technology 15, 506–518.

Pozzato, G., Formentin, S., Panzani, G., Savaresi, S.M., 2018. Least costly energy management for extended range electric vehicles with start-up characterization, in: 2018 IEEE Conference on Control Technology and Applications (CCTA), IEEE. pp. 1020–1025.

Pozzato, G., Formentin, S., Panzani, G., Savaresi, S.M., 2019. Least costly energy management for extended-range electric vehicles with noise emissions characterization, in: 9^{th} International Symposium on Advances in Automotive Control, IFAC.

Pozzato, G., Formentin, S., Panzani, G., Savaresi, S.M., 2020. Least costly energy management for extended-range electric vehicles: an economic optimization framework. European Journal of Control .

Rajamani, R., 2011. Vehicle dynamics and control. Springer Science & Business Media.

Roberts, A., Brooks, R., Shipway, P., 2014. Internal combustion engine cold-start efficiency: A review of the problem, causes and potential solutions. Energy Conversion and Management 82, 327–350.

Sciarretta, A., Guzzella, L., 2007. Control of hybrid electric vehicles. IEEE Control systems 27, 60–70.

Serrao, L., Onori, S., Sciarretta, A., Guezennec, Y., Rizzoni, G., 2011. Optimal energy management of hybrid electric vehicles including battery aging, in: American Control Conference (ACC), 2011, IEEE. pp. 2125–2130.

Sundstrom, O., Guzzella, L., 2009. A generic dynamic programming matlab function, in: Control Applications, (CCA) & Intelligent Control,(ISIC), 2009 IEEE, IEEE. pp. 1625–1630.

Suri, G., Onori, S., 2016. A control-oriented cycle-life model for hybrid electric vehicle lithium-ion batteries. Energy 96, 644–653.

Walpole, S.C., Prieto-Merino, D., Edwards, P., Cleland, J., Stevens, G., Roberts, I., 2012. The weight of nations: an estimation of adult human biomass. BMC public health 12, 439.

Warner, J.T., 2015. The Handbook of Lithium-Ion Battery Pack Design: Chemistry, Components, Types and Terminology. Elsevier.

Xiong, W., Zhang, Y., Yin, C., 2009. Optimal energy management for a series–parallel hybrid electric bus. Energy conversion and management 50, 1730–1738.

Zanon, M., Grüne, L., Diehl, M., 2017. Periodic optimal control, dissipativity and MPC. IEEE Transactions on Automatic Control 62, 2943–2949.

Zwicker, E., Fastl, H., 2013. Psychoacoustics: Facts and models. volume 22. Springer Science & Business Media.